68th International Astronautical Congress (IAC), Adelaide, Australia, 25-29 September 2017.

IAC-17,B2,3,1,x38151

GNSS/INS/Star Tracker Integration for Real-Time On-Board Autonomous Orbit and Attitude Determination in LEO, MEO, GEO and Beyond

Vincenzo Capuano, Endrit Shehaj, Cyril Botteron, Paul Blunt, Pierre-André Farine
École Polytechnique Fédérale de Lausanne (ESPLAB), Switzerland, vincenzo.capuano@epfl.ch

Abstract

In our previous studies, we demonstrated that Global Navigation Satellite System (GNSS) signals can be processed, not only in Low Earth Orbit (LEO), but also in higher earth orbits, up to the Moon. In order to maximize the GNSS-based navigation performance, we implemented an adaptive orbital filter, which fuses the GNSS observations with a model of the spacecraft dynamics, achieving a navigation accuracy of approximately 100 meters, at Moon altitude. In this paper, we take a step forward and we investigate the design of an advanced multisensor solution that, in addition to combining GNSS with an orbital forces model, also adds the integration of an Inertial Navigation System (INS) and of a Star Tracker, in order to provide a versatile, real-time, on-board, autonomous orbit and attitude determination in different space mission scenarios, from LEO to GEO and beyond.

First, we describe the designed architecture of the integrated system, then its implementation, and finally we report its achieved navigation performance for different altitudes up to the Moon, showing that the synergistic integration of the different sensors, can overcome their individual drawbacks and provide a better navigation performance than either could achieve individually.

Keywords: GNSS, INS, Star Tracker, Orbit Determination, Navigation, Attitude Determination

1. Introduction

A synergistic integration of different metrology systems can overcome the individual limitations of each of them and provide a more accurate and robust navigation solution. This is particularly suited for spacecraft applications that demand highly precise and accurate autonomous navigation while requiring robustness, versatility, and adaptability to different scenarios and orbits from Low Earth Orbits (LEOs), Medium Earth Orbits (MEOs), to Geosynchronous Orbits (GEOs) and beyond.

In our previous studies at EPFL ESPLAB [1], [2], [3], [4] [5], [6] as well as in other studies in the current literature as [7], [8], [9] and [10], the use of Global Navigation Satellite Systems (GNSSs), already successfully used in LEO, has been assessed also in higher Earth orbits, well above the GNSS constellations, up to the Moon altitude. A GNSS-based navigation appears a very attractive solution, since it can maximize the autonomy of the spacecraft, reducing the cost of ground operations and allows for budget-limited missions of micro- and nanosatellites. In [3], we described the successful realization of a GPS L1 C/A spaceborne receiver proof-of-concept, able to process signals up to the Moon altitude. In [4], we presented an adaptive GNSS-based orbital filter, which can significantly improve the navigation accuracy at the Moon altitude down to 50-200 m (otherwise of several km if not filtered), by fusing GNSS observations with orbital forces models. In this study, we make a further step forward in the same line of research, by investigating a more advanced multisensor architecture that, in addition to combining GNSS with an orbital forces model, it also adds the integration of an Inertial Navigation System (INS) and of a Star sensor. The resulting integrated system provides versatile, robust, real-time, on-board, autonomous navigation in different mission scenarios, from LEO to GEO and beyond (up to the Moon). The integration of INS and Star sensor with the GNSS, enables both orbit and attitude determination, therefore the full kinematic state.

The paper is organized as follows. Section 2 introduces the simulation models and assumption of the study. Section 3 describes the preliminary architecture and

implementation of the GNSS/INS/Star Tracker integration. Section 4 presents the orbit and attitude determination performance and in Section 5 the conclusions are drawn.

2. Simulation models and assumptions

2.1. Spacecraft kinematics and dynamics

As specified in the title of this paper, as well as in the abstract, the proposed integrated navigation system is conceived to provide navigation in the space volume between Low Earth Orbit (LEO) and the Moon altitude, therefore being suitable to navigate in LEO, MEO, Geosynchronous Earth Orbit (GEO) and High Earth Orbit (HEO) up to the Moon (on average ~384000 km far away from Earth). Let us name this volume "Extended Space Service Volume" (ESSV) to distinguish it from what is known as GPS Space Service Volume (SSV), defined in [11] as the volume between the altitudes 3000 km (LEO) and 36000 km (GEO). In our study, tests and verifications of the achievable navigation performance were performed for each of these considered orbits, however, in this paper (see Section 4), in order to summarize and avoid repetitions of similar results, only the results obtained for a highly elliptical direct Earth-Moon Transfer Orbit (MTO) are presented, which, in terms of GNSS signals conditions are well representative of the scenario encountered in the whole ESSV.

Figure 2:1 illustrates the full trajectory from LEO to the Moon. For this analysis we considered the elliptical MTO (in light blue), as well as a short trajectory in LEO (in yellow) followed by a burn required to bring the spacecraft into the MTO.

The initial translational kinematic state, for the MTO, is defined in Table 2:1. Then, the full orbit was generated using the Astrogator tool of STK software [12], in order to obtain the highest possible accuracy, propagating the initial orbit and attitude condition as function of all the orbital and attitude perturbations. The LEO portion is characterized by a $\Delta \boldsymbol{V} = [2.9287534,\ 1.0264705,\ 0.491906]$ km/s with respect to Earth Centered Inertial (ECI) frame.

The kinematics for the full MTO trajectory was converted to a user vehicle motion file (Spirent-compatible format) and used as reference for the Spirent simulator to simulate and generate realistic RF GNSS signals, used in this study for simulation tests presented in Section 4 and later for hardware-in-the-loop experiments.

Table 2:1 Translational kinematic state at the beginning of the MTO.

Parameters	Values
ECI initial position (km):	$\begin{bmatrix} 2405.932950295456 \\ -5294.449058153414 \\ -3021.365507500000 \end{bmatrix}$
ECI initial velocity (km/s):	$\begin{bmatrix} 10.190645136091339 \\ 3.593586746431558 \\ 1.722103380700000 \end{bmatrix}$
Departure date:	1st Jul 2005, 18:41:38
Final date:	6th Jul 2005, 05:11:12

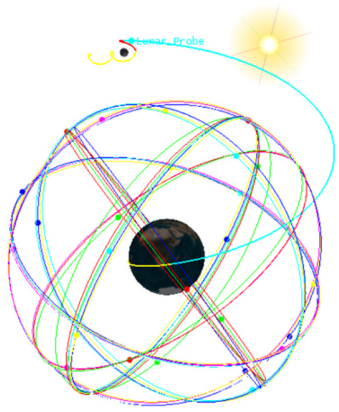

Figure 2:1 Full trajectory from Earth to Moon.

2.2. GNSS

Assumed Receiver characteristics

For this study, we assumed the specifications of a spaceborne receiver currently under development in our laboratory, the *SANAG* (Spaceborne Autonomous Navigation based on GNSS) receiver [13], specifically conceived for autonomous GNSS-based orbit determination in the ESSV. The main characteristics of the assumed receiver, relevant for the presented study, are summarized in Table 2:2.

Table 2:2 SANAG receiver characteristics.

Processed Signals:	GPS L1 C/A, GPS L5
Acquisition Sensitivity:	15 dB-Hz with Doppler assistance for L1 C/A (from the navigation filter)
Tracking Sensitivity:	12 dB-Hz and 15 dB-Hz with Doppler assistance (from the orbital filter) for L5Q and L1 C/A, respectively
L1 C/A Acquisition and Synchronization time:	5 min above 20 dB-Hz 10 min from 15-20 dB-Hz
Antenna max gain	10 dBi

As reported in Table 2:2, the receiver has the capability of processing two GPS signals' frequencies: L1 and L5. The processing of the L1 C/A signal is always assumed for the acquisition engine (otherwise the primary code chipping rate of the L5 signal , being 10 times higher than the one of the L1 signal, would cause a significantly longer acquisition processing). Afterwards, once the L1 C/A is acquired, also GPS L5Q can be tracked, by exploiting the frequency relation between L1 and L5 and their code synchronization.

Note that, to preserve the complete autonomy from external information/augmentations, for the SANAG receiver we only considered code-based GNSS observations (and not carrier-phase-based). In fact, while more accurate, the processing of carrier phase-based observations requires additional information not integral part of the GNSS data message.

GNSS constellation and signals

The GPS constellation was modelled according to the almanac of the 1st July 2005 that includes a total of 29 satellites (PRN from 1 to 31 except 12 and 17)).

In our performed simulations, we made use of the Spirent GSS8000 to reproduce realistic GPS signals, exactly as the one that would be present at the receiver's antenna, in the assumed MTO.

Taking into account gain patterns of both transmitter and receiver antennas and free space signal propagation losses, the signal power levels received at the receiver's antenna position were modelled as in equation (1) of our previous study [1], according to the guaranteed minimum received signal power (see [14] and [15]) for both GPS signals considered.

In order to track very weak signals up to the Moon, we assumed to always be able to have 10 dB gain at the receiver antenna, independently of the spacecraft attitude, using a steerable antenna or more than one antenna on different faces of the spacecraft. More details about this assumption can be found in [16].

In order to account for the signals transmitted by the side lobes of the transmitters, 3D receiver and transmitters' antenna patterns for each satellite of the constellation were modeled. More details about the assumed transmitters' antenna patterns can be found in [16].

Note that although only the GPS constellation and signals are considered in this study, the results of Section 4 are extendible also to the case of other constellations, or to the case of combined constellations for which better availability and thus better GDOP and performance can be reached.

GNSS observations

The code-based GNSS observations were modelled exactly as described in our previous study [6], accounting for transmitters' clock error and broadcast ephemeris error, atmospheric delay, multipath effect and receiver errors. A specific strategy (described in our previous study [6]) was developed to deal with possible ionospheric delays. According to [17], we considered a standard deviation value of 0.5 m for transmitter's clock and broadcast ephemeris errors, a standard deviation of 0.2 m for possible multipath [18]. As done in [19], the receiver error was modeled as function of the receiver characteristics and of the carrier-to-noise-ratio C/N_0 to account for the large variations of the signals power level at the receiver position in the ESSV.

2.3 INS and Star Tracker

Since the goal of this study was to only demonstrate the fusion of INS and Star Tracker with the SANAG receiver and simulate the resultant integrated solution, we did not develop any specific Inertial Measurement Unit (IMU) or Star Tracker. Therefore, simplified Matlab models were used to only test the multi-sensor fusion in post-processing mode on a computer.

Tactical grade accelerometers and gyros were assumed for the modelled IMU, as a reasonable compromise between performance, dimensions and cost. The specifications assumed for the accelerometers and for the gyros are respectively reported in Table 2:3, according to [20] and in Table 2:4 according to [21].

As suggested in [21], a Star Tracker typically produces errors along the boresight axis of an order of magnitude larger than the other axes. However, if two Star Trackers are used placed orthogonal to each other, their combined attitude estimation has a nearly isotropic error. As in the example 6.1 of [21], a simplified Star Tracker model is assumed that provides every second k, a quaternion measurement with a covariance $R_k = 36I_3$ arcsec^2.

Table 2:3 Accelerometers characteristics [20].

Accelerometer biases x,y,z (μg):	$[900 \quad -1300 \quad 800]$
Accelerometer scale factor and cross coupling errors (ppm):	$\begin{bmatrix} 500 & -300 & 200 \\ -150 & -600 & 250 \\ -250 & 100 & 450 \end{bmatrix}$
Accelerometer noise root PSD $\left(\mu g/\sqrt{\text{Hz}}\right)$	100
Accelerometer quantization level (m/s^2)	$1 \cdot 10^{-2}$

Table 2:4 Gyros characteristics [21].

Initial Gyro biases (°/h):	$[0.1 \quad 0.1 \quad 0.1]$
Gyro scale factor and cross coupling errors (ppm):	$\begin{bmatrix} 1500 & 1000 & 1500 \\ 500 & 1000 & 2000 \\ 1000 & 1500 & 1500 \end{bmatrix}$
Gyro noise parameters:	$\sigma_u = \sqrt{10} \times 10^{-10}\ rad/s^{3/2}$ $\sigma_v = \sqrt{10} \times 10^{-7}\ rad/s^{1/2}$ $\sigma_s = \sigma_U = \sigma_L = 0$

3. GNSS/INS/Star Tracker Integration

3.1. Preliminary architecture

Figure *3:1* illustrates the preliminary architecture of the proposed GNSS/INS/Star Tracker integration.

For the orbit determination, position and velocity vectors of the spacecraft are estimated by fusing the GNSS observations with the inertial solution and the dynamic solution, obtained respectively from the INS and from an orbital forces model. When the accelerometers are enough sensitive to provide a nonzero measurement (for the assumed IMU essentially this happens in LEO, in presence of strong atmospheric resistance and during powered flight), the total acceleration acting on the spacecraft is a combination of the measured non gravitational acceleration and the accurately modelled gravitational acceleration due to Earth, Sun and Moon. More in details, collected GNSS pseudoranges and pseudorange rates are fused by means of a sequential filter with their dynamic and inertial prediction. As illustrated in Figure *3:1*, the integrated navigation solution is used to aid the signal processing modules of the GNSS receiver, otherwise not able to acquire and track the very weak signals in the higher altitudes of the ESSV, when also affected by large Doppler and Doppler rates. The aiding process adopted is well described in our previous research [22].

The attitude is determined by integrating the gyros observations (angular velocities) with the Star Tracker attitude estimation. The angular velocities are used to propagate the previous estimate, which is fused with the current attitude observation provided by the Star Tracker.

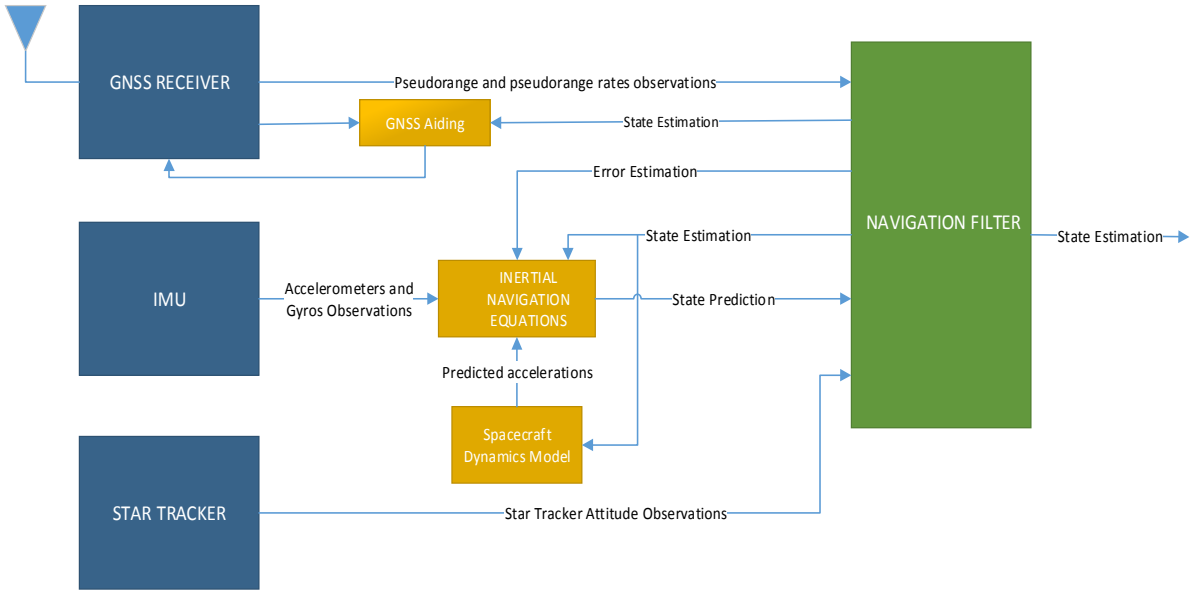

Figure 3:1 GNSS/INS/Star Tracker Integration Preliminary architecture.

3.2. Preliminary implementation

In this first preliminary implementation, orbit determination and attitude determination are addressed separately. In a second step they will be combined into a single estimator. For both orbit and attitude determination, as compromise between accuracy and computational burden (to be minimized for on-board navigation), the Extended Kalman Filter (EKF) algorithm has been adopted in our implementation as estimation method, since it does not need to store and compute large amount of past data.

For the orbit determination, the state vector includes position and velocity vector of the spacecraft, clock bias and drift estimation of the GNSS receiver and empirical accelerations, as in the implementation of our previously developed GNSS-based orbital filter, well described in our previous research paper [23]. Unlike in the standard reduced dynamic approach adopted in [23], here the empirical accelerations, also account for the accelerometers biases.

In order to reduce the computational weight, the spacecraft dynamics model used to propagate the filter estimate, includes different combinations of forces and different levels of details at different altitude intervals, as reported in Table 3:1, where: $\boldsymbol{r}$ is the position vector, $\boldsymbol{a_g}$ is the acceleration due to Earth's gravity, $\boldsymbol{a_s}$ is the acceleration due to the Sun, $\boldsymbol{a_m}$ is the acceleration due to the Moon, $\boldsymbol{a_{srp}}$ is the acceleration due to solar radiation pressure.

A detailed description of each adopted orbital forces' implementation, can be found in [5].

Table 3:1 Orbital forces modelled.

Altitude	Modelled Perturbations
$\boldsymbol{r < 9600\ km}$	$-\ \boldsymbol{a_g}$ with spherical harmonics of Earth gravitational potential up to 6th degree and 6th order
$\boldsymbol{9600\ km \leq r \leq 50\ 000\ km}$	- $\boldsymbol{a_g}$ with spherical harmonics up to 2nd degree and 2nd order - $\boldsymbol{a_{srp}}$ - $\boldsymbol{a_m}$ and $\boldsymbol{a_s}$
$\boldsymbol{r > 50\ 000\ km}$	- $\boldsymbol{a_g}$, only 1st order - $\boldsymbol{a_{srp}}$ - $\boldsymbol{a_m}$ and $\boldsymbol{a_s}$

In the integration filter, the GNSS observations are predicted by means of equation (15) of [23], using position and velocity of the GPS satellites (computed by using the transmitted ephemeris), the predicted user's position and velocity vectors as well as predicted receiver's clock offset and drift. Predicted user's position and velocity vectors are computed by integrating the dynamics of the spacecraft:

$$\boldsymbol{a}(\boldsymbol{r},t) = \boldsymbol{a_g}(\boldsymbol{r},t) + \boldsymbol{a_s}(\boldsymbol{r},t) + \boldsymbol{a_m}(\boldsymbol{r},t) + \boldsymbol{a_{srp}}(\boldsymbol{r},t) + \boldsymbol{a_{um}}(\boldsymbol{r},t) + \boldsymbol{a_{emp}} \quad (3:1)$$

Where, $\boldsymbol{a_{um}}$ is any unknown un-modeled acceleration (e.g. atmospheric resistance in LEO and a burn during maneuvers) and $\boldsymbol{a_{emp}}$ is the empirical acceleration that takes into account any residual acceleration. While $\boldsymbol{a_g}$, $\boldsymbol{a_s}$, $\boldsymbol{a_m}$, $\boldsymbol{a_{srp}}$ are modelled in the spacecraft dynamics, $\boldsymbol{a_{um}}$ is measured by the accelerometers. In addition, as in [23], empirical accelerations $\boldsymbol{a_{emp}}$, modelled as first order, stationary, Gauss-Markov process are also integrated to compensate for un-modeled and miss-modeled forces, not sensed by the accelerometers. Unlike in our previous implementation [23], here, the accelerometers are used to autonomously navigate also in case of unknown accelerations, not modelled in the spacecraft dynamics, with a resultant increased robustness against unknown non gravitational perturbing event.

It is important to mention that, in order to dynamically weight GNSS observations over time (for different altitudes up to the Moon), whose accuracy is strongly variable (due to decreasing signal power at the receiver position and increasing GDOP), an adaptive tuning of the covariance matrix of the measurement is adopted. Also the covariance matrix of the process is updated for each orbital forces combination reported in Table 3:1. This strategy allows for an effective filtering in the whole ESSV, from LEO to the Moon altitude, in drastically different signal and user/transmitters geometry conditions [23]. In addition, although in principle unknown accelerations can be sensed by the accelerometers and accounted in the orbit propagation, an additional countermeasure is to increase the weight of the GNSS observations (if available) when the acceleration sensed by the accelerometers is higher than a threshold. Therefore, the filter tuning is also function of the accelerometers output.

For the attitude determination, a sequential 15-state EKF was implemented according to the formulation proposed in Table 6.1 of [21], where, as well as the attitude, also all gyro calibration parameters are estimated (3 biases, 3 scale factors and 6 misalignments). Note that once the calibration parameters are estimated and smoothed, a 6-state EKF can be used, where only the attitude and the gyros biases are estimated.

4. Preliminary simulated performance

4.1. Orbit determination

Figure 4:1 displays the accuracy in position and velocity determination (respectively the norm of the 3D position error vector and of 3D the velocity error vector) if a single-epoch least-squares estimator based on the available GPS measurements is used; errors larger than 5 km in positioning and larger than 2 km/s in velocity estimation make the unfiltered solution almost meaningless for many applications. The same estimation errors when using the GNSS/INS/Star Tracker based orbital filter are illustrated in Figure 4:2. For the modelled orbit and receiver assumptions describe above, the improvement in accuracy is extremely evident: at the Moon altitude, the error in positioning does not exceed 30 m, while in velocity estimation is smaller than 3 cm/s.

Table 4:1, Table 4:2, Table 4:3 and Table 4:4 report the statistics computed in terms of standard deviation (1 σ) of the error for the Radial, In-Track and Cross-Track components, for different portions of the MTO, respectively in LEO (altitude h ≤ 2000 km), in MEO and GEO (2000 < h ≤ 36000 km), in HEO for 36000 < h ≤100000 km and for 100000 < h ≤384400 km. In the same tables also standard deviation and the mean are reported for the 3D position and velocity error vectors.

Although the GNSS observations were modeled accurately, it is important to be aware that these results were obtained in simulation and may differ from hardware-in-the-loop tests results, where it is likely that other sources of error will be present.

In order to evaluate the robustness against unexpected high dynamics, we tested the performance during un-modelled and unknown accelerations of two different orders of magnitude and two different durations. We considered the accelerations required to provide the $\Delta\boldsymbol{V}$ defined in Section 2.1, respectively in 100 and 10 s. Figure 4:3 and Figure 4:4 display the position and velocity determination errors during these three accelerations respectively, when using the previously implemented GNSS based orbital filter [23] and when using the GNSS/INS/Star Tracker based orbital filter proposed here. As already specified, the accelerations are assumed to be unknown and un-modeled in the spacecraft dynamics. We can see an improved performance are obtained in position estimation and most of all in velocity estimation when using the integration of GNSS/INS/Star Tracker. The benefit of using the integration of the three metrology systems is

more evident for the strongest acceleration (see Figure 4:4), where both position and velocity estimations based on only GNSS are significantly degraded during the acceleration; however thanks to the measurements provided by the accelerometers the GNSS/INS/Star Tracker orbital filtered solution appears significantly less affected, showing a considerable smaller error.

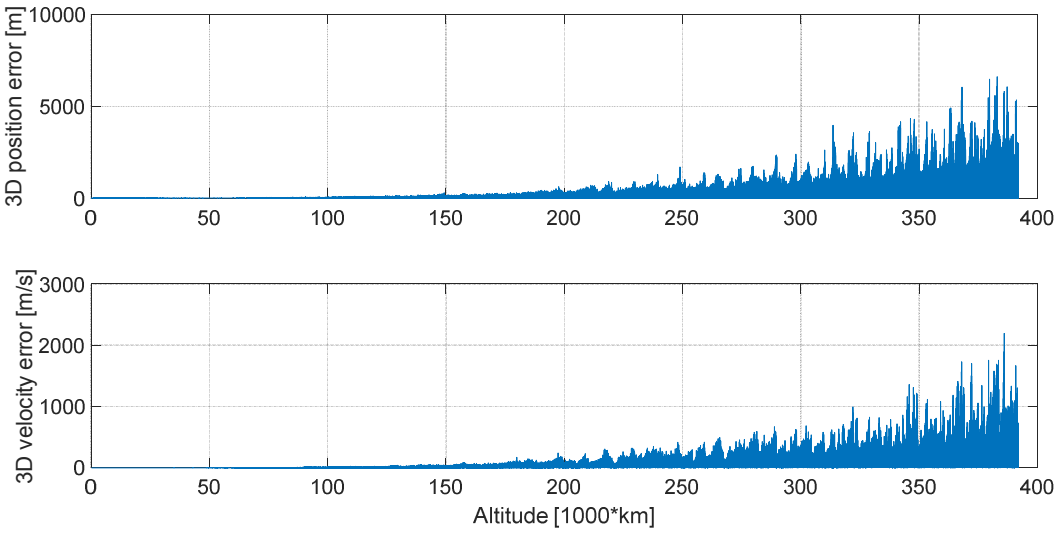

Figure 4:1 Norm of the 3D position error vector and of 3D the velocity error vector when using a single-epoch least-squares estimator based on the available GPS measurements.

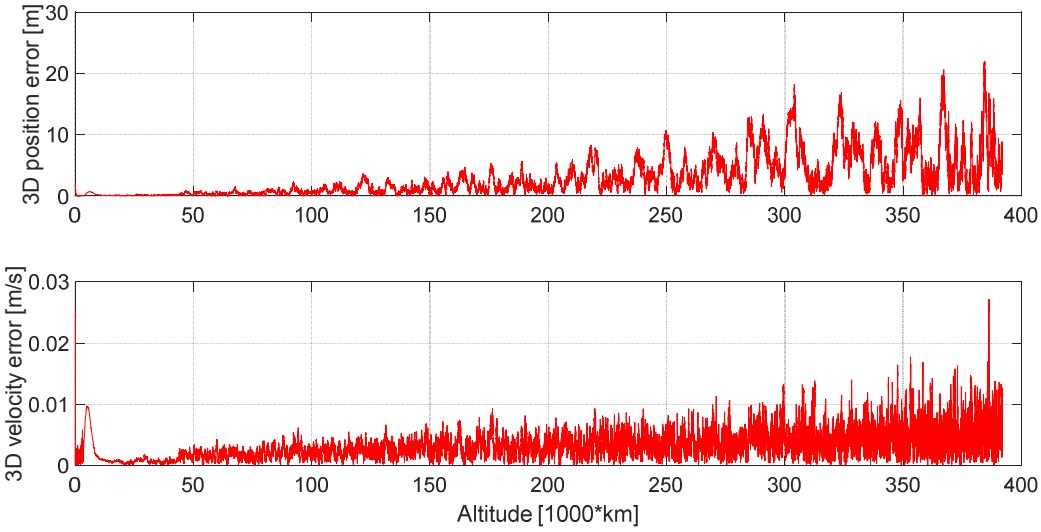

Figure 4:2 Norm of the 3D position and velocity errors when using the GNSS/INS/Star Tracker based orbital filter..

Table 4:1 Statistics of the orbit determination solution error in LEO ($h \leq 2000$ km).

Method	State component	Radial	In-track	Cross-track	Norm	
		std	std	std	std	mean
GPS only (single-epoch least square)	Position (m)	0.733	0.482	0.405	0.550	0.795
	Velocity (cm/s)	0.13	0.08	0.07	0.07	0.15
GPS/INS/Star Tracker based Orbital Filter	Position (m)	0.035	0.058	0.052	0.052	0.071
	Velocity (cm/s)	0.10	0.08	0.07	0.06	0.13

Table 4:2 Statistics of the orbit determination solution error in MEO and GEO ($2000 < h \leq 36000\ km$).

Method	State component	Radial	In-track	Cross-track	Norm	
		std	std	std	std	mean
GPS only (single-epoch least square)	Position (m)	1.036	0.261	0.246	0.759	0.790
	Velocity (cm/s)	8.04	2.01	1.94	6.94	4.93
GPS/INS/Star Tracker based Orbital Filter	Position (m)	0.085	0.184	0.053	0.147	0.162
	Velocity (cm/s)	0.09	0.22	0.05	0.21	0.15

Table 4:3 Statistics of the orbit determination solution error in HEO for $36000 < h \leq 100000$ km.

Method	State component	Radial	In-track	Cross-track	Norm	
		std	std	std	std	mean
GPS only (single-epoch least square)	Position (m)	10.806	0.811	0.857	7.519	7.850
	Velocity (cm/s)	192.41	16.57	19.11	146.01	127.84
GPS/INS/Star Tracker based Orbital Filter	Position (m)	0.497	0.201	0.266	0.334	0.502
	Velocity (cm/s)	0.09	0.11	0.145	0.09	0.18

Table 4:4 Statistics of the orbit determination solution error in HEO for $100000 < h \leq 384400$ km.

Method	State component	Radial	In-track	Cross-track	Norm	
		std	std	std	std	mean
GPS only (single-epoch least square)	Position (m)	608.254	11.459	10.905	469.088	387.530
	Velocity (cm/s)	17326.4	361.7	386.4	13264.1	11160.2
GPS/INS/Star Tracker based Orbital Filter	Position (m)	6.253	0.807	0.849	3.972	5.012
	Velocity (cm/s)	0.38	0.19	0.19	0.23	0.41

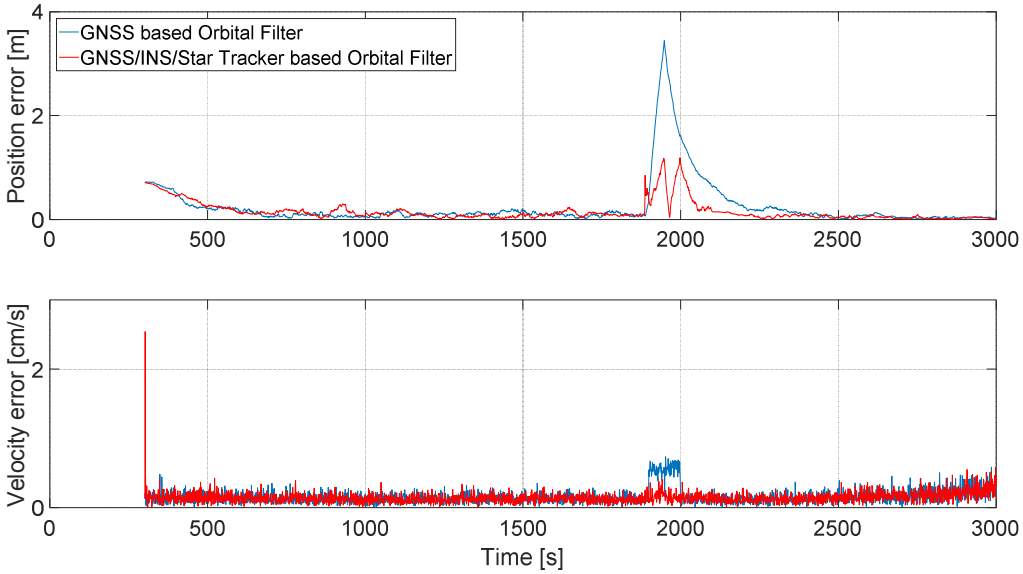

Figure 4:3 Position and velocity error vectors norm, during 100 s of the un-modelled unknown acceleration $\boldsymbol{a}_{\Delta V} = [29.287534,\ 10.264705, 4.91906]$ *m/s² in LEO.*

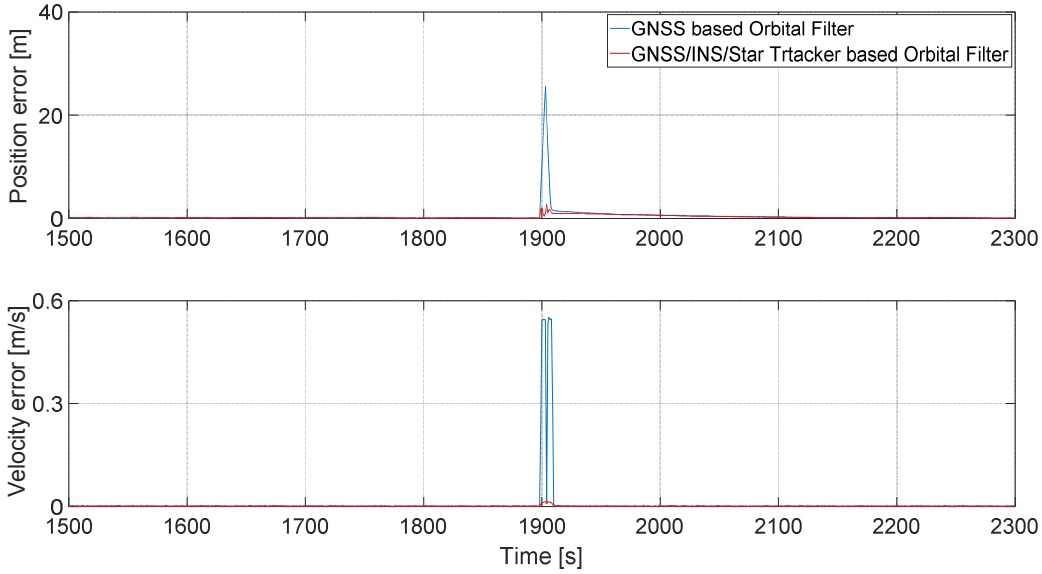

Figure 4:4 Position and velocity error vectors norm, during 10 s of the un-modelled unknown acceleration $\boldsymbol{a}_{\Delta V} = [292.87534,\ 102.64705, 49.1906]$ *m/s² in LEO.*

4.2. Attitude determination

Figure 4:5 displays the attitude determination error expressed in terms of Roll, Pitch and Yaw, when only the Star Tracker is used, when only the gyros are used and when this is fused with the gyros. For all three Roll, Pitch and Yaw, when fusing the Star Tracker with the gyros observations, the standard deviation of about 30 μrad (1σ) of the Star Tracker is reduced of approximately one order of magnitude (see red and blue curve in Figure 4:5). The convergence of the filter lasts only a few tens of seconds, as shown in Figure 4:6. While, as expected, a typical drifting error characterizes the attitude determination based on only gyros (green curve in Figure 4:5).

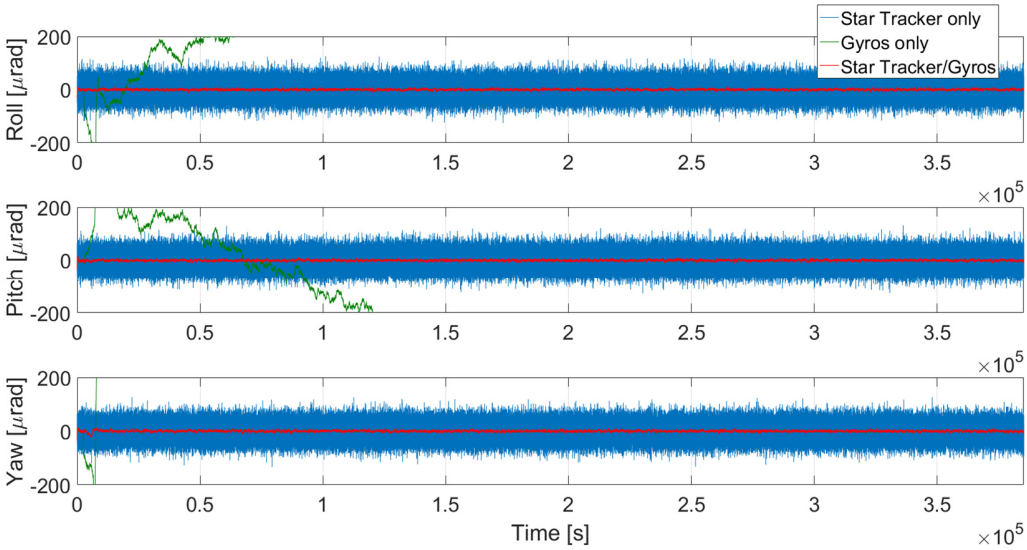

Figure 4:5 Attitude determination error.

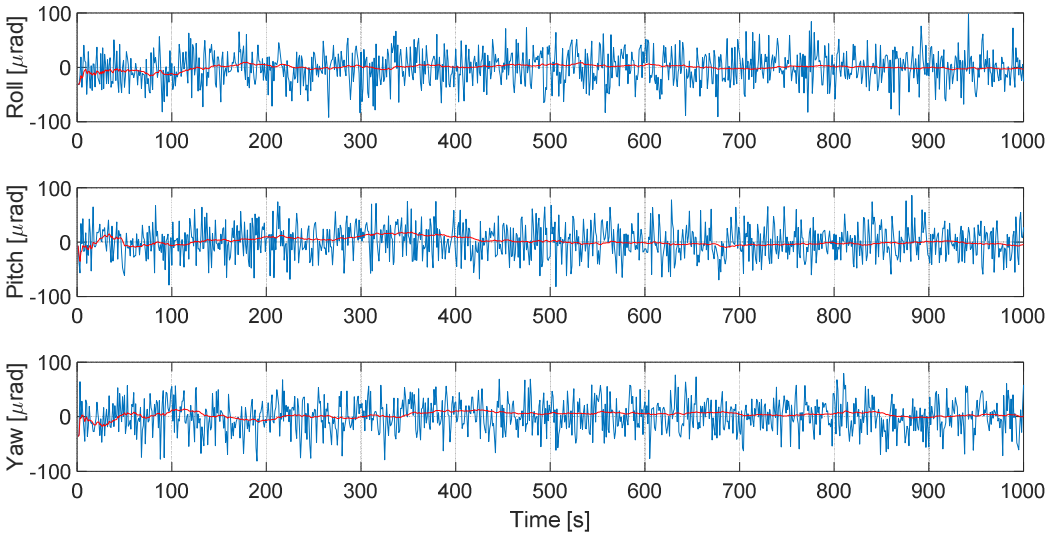

Figure 4:6 Zoom of the attitude determination error in the first 1000s.

5. Conclusions

The research study presents a preliminary GNSS/INS/Star Tracker integration for on-board autonomous orbit and attitude determination in LEO, MEO, GEO and HEO and beyond up to the Moon altitude. The proposed solution follows the development of a GPS L1/L5 receiver proof of concept, specifically designed in our laboratory (ESPLAB of EPFL) for autonomous navigation from LEO to the Moon and therefore within the defined ESSV. Our previously implemented GNSS based orbital filter, able to maximize the accuracy in orbit determination, is combined with additional observations provided by an IMU and a Star Tracker, in order to increase the robustness against un-modeled and unknown accelerations and also to provide attitude determination, as well as orbit determination. With respect to a traditional unfiltered GNSS-only single epoch least square solution, preliminary simulations of the achievable navigation performances show that a considerable accuracy improvement can be obtained in position and velocity determination, in the whole ESSV. During the full considered MTO, the maximum positioning error is lower than 30 m, while the velocity determination error does not exceed 3 cm/s. Other preliminary simulations results confirm that the integration of INS to the GNSS unit, can reduce the degradation of the autonomous orbit determination performance during an un-modeled unknown acceleration.

A preliminary attitude determination strategy is introduced, which relies on the Star Tracker attitude measurements and on the gyros attitude rates measurements. Also in this case, the already very accurate Star Tracker attitude estimation accuracy is further improved down to $3\,\mu rad\ (1\sigma)$.

Future works will aim at improving the models of INS and Star Tracker and the integration architecture. In addition, hardware-in-the-loop tests will be performed to assess the effective performances.

References

[1] V. Capuano, C. Botteron and P.-A. Farine, "GNSS Performances for MEO, GEO and HEO," in *64th International Astronautical Congress*, Beijing, China, 2013.

[2] V. Capuano, C. Botteron, Y. Wang, J. Tian, J. Leclère and P. A. Farine, "Feasibility Study of GNSS as Navigation System to Reach the Moon," *Acta Astronautica,* vol. 116, pp. 186-201, 2015.

[3] V. Capuano, P. Blunt, C. Botteron, J. Tian, J. W. Y. Leclere, F. Basile and P.-A. Farine, "Standalone GPS L1 C/A Receiver for Lunar Missions," *Sensors,* vol. 16, no. 3, pp. 347-368, March 2016.

[4] V. Capuano, F. Basile, C. Botteron and P.-A. Farine, "GNSS Based Orbital Filter for Earth Moon Transfer Orbits," *Journal Of Navigation,* pp. 1-20, 2015.

[5] V. Capuano, "GNSS-Based Navigation for Lunar Missions," École polytechnique fédérale de Lausanne (PhD thesis), Lausanne, 2016.

[6] V. Capuano, E. Shehaj, C. Botteron, P. Blunt, B. Wang and P.-A. Farine, "Availability and ranging error analysis for a GPS L1/L5 receiver navigating to the Moon," in *European Navigation Conference (ENC 2017)*, Lausanne, Switzerland, 2017.

[7] L. Mususmeci, F. Dovis, J. S. Silva, P. F. Silva and H. D. Lopes, "Design of a High Sensitivity GNSS receiver for lunar missions," *Advances in Space Research,* 2016.

[8] G. B. Palmerini, M. Sabatini and G. Perrotta, "En route to the Moon using GNSS signals," *Acta Astronautica,* vol. 64, 2009.

[9] P. F. Silva, H. D. Lopes, T. R. Peres, J. S. Silva, J. Ospina, F. Cichocki, F. Dovis, L. Musumeci, D. Serant, T. Calmettes, I. Pessina and J. V. Perello, "Weak GNSS Signal Navigation to the Moon," in *ION GNSS+*, Nashville, Tennessee, USA, 2013.

[10] M. Manzano-Jurado, J. Alegre-Rubio, A. Pellacani, G. Seco-Granados, J. Lopez-Salcedo, E. Guerrero and A. Garcia-Rodriguez, "Use of weak GNSS signals in a mission to the moon," in *Satellite Navigation Technologies and European Workshop on GNSS Signals and*

Signal Processing (NAVITEC), 7th ESA Workshop on, 2014.

[11] J. Miller, "Enabling a Fully Interoperable GNSS Space Service Volume," in *6th International Committee on GNSS (ICG)*, Tokyo, Japan, 2011.

[12] AGI, "STK HPOP," [Online]. Available: http://www.agi.com/resources/help/online/stk/10.1/index.html?page=source%2Fhpop%2Fhpop.htm. [Accessed 24 August 2016].

[13] P. Blunt, C. Botteron, V. Capuano, S. Ghamari, M. Rico and P.-A. Farine, "Ultra-high sensitivity state-of-the-art receiver for space applications," in *ESA NAVITEC 2016*, Noordwijk, Netherlands, 2016.

[14] "ICD-GPS-200H Navstar GPS Space Segment / User Segment Interfaces," 2013.

[15] "ICD-GPS-705C Navstar GPS Space Segment/User Segment L5 Inter-faces," 2012.

[16] E. Shehaj, V. Capuano, V. Botteron, P. Blunt and P.-A. Farine, "GPS based navigation performance analysis within and beyond the Space Service Volume for different transmitters' antenna patterns," *Aerospace,* vol. 4, no. 3, 2017.

[17] K. D. McDonald and C. Hegarty, "Post-Modernization GPS Performance Capabilities," in *Proceedings of the IAIN World Congress and the 56th Annual Meeting of The Institute of Navigation*, San Diego, CA, 2000.

[18] H. C. Kaplan E.D., Understanding GPS principles and applications, Artech House, 2006.

[19] V. Capuano, E. Shehaj, P. Blunt, C. Botteron and P.-A. Farine, "High accuracy GNSS based navigation in GEO," *Acta Astronautica,* vol. 136, pp. 332-241, 2017.

[20] P. D. Groves, Principles of GNSS, Inertial, and Multisensor Integrated Navigation systems, Artech House, 2013.

[21] F. L. Markley and J. L. Crassidis, Fundamentals of Spacecraft Attitude Determination and Control, Springer, 2014.

[22] V. Capuano, P. Blunt, C. Botteron and P.-A. Farine, "Orbital filter aiding of a high sensitivity GPS receiver for lunar missions," *Navigation,* 2017.

[23] V. Capuano, E. Shehaj, P. Blunt, C. Botteron and P.-A. Farine, "An adaptive GNSS-based reduced dynamic approach for real time autonomous navigation from the Earth to the Moon," in *Pacific PNT 2017*, Honolulu, HI, 2017.